Engineering and Technology Journal
Journal homepage: https://etj.uotechnology.edu.iq

Experimental investigation of exhaust temperature effect on TEG cells power generation and assessment of engine SFC and emissions

Eid S. Mohamed

Faculty of Engineering, Mechanical Eng. Dept., Al-Baha University, Alaqiq, Saudi Arabia.
Faculty of Engineering, Automotive Dept., Helwan University, Egypt.

*Corresponding author Email: e.mohamed@bu.edu.sa

HIGHLIGHTS

- The impact of a thermoelectric generator (TEG) arrangement on engine manifold performance was analyzed
- Electrical power generation with forty TEGs was detailed, highlighting system efficiency and energy output
- Comparisons of BSFC were made for engine operation with and without active TEGs for performance assessment
- Results showed lower emissions in engines equipped with active TEGs, suggesting environmental benefits

Keywords:
Exhaust temperature; Thermoelectric cell; Electrical power generation; BSFC; Emissions.

ABSTRACT

The thermoelectric cell generators (TECG) convert thermal power into electrical power generated. The main factor in its operation is the temperature difference (TD) between its surfaces. An experimental investigation was conducted into the waste heat recovery performance of the TECG system. Forty thermoelectric cells (TECs) are supported on the (4×5) upper and (4×5) lower and upper arrangement of the engine exhaust manifold. The electrical power generated (EPG), exhaust gas flow rate, exhaust temperature, brake-specific fuel consumption (BSFC), and exhaust emissions were experimentally investigated under different engine speeds and 50 N.m and 100 N.m engine load conditions. Comparative results of the BSFC and emissions have ben measured with and without the TECG system. Experimental results observed that the maximum power values generated are approximately 218.5 W by TECG. An engine BSFC has been reduced by (2.56%:2.89%) under the TECG. The results show the improvement of CO is approximately 1.92% and 5.12% with the TECG system at loads 50 N.m and 100 N.m, respectively, and CO_2 emission improvement by 4.32% and 4.52% with the TECG system throughout the speed range and two engine loads. The proposed TECG system, supported by a gasoline engine, is effective under high engine speed and load.

1. Introduction

The thermoelectric cell generators (TECG) are based on the thermoelectric effect principles, which involve converting heat into electricity. One significant aspect is the exhaust temperature and its impact on power generation. Evaluating the relationship between exhaust temperature and electrical power generated (EPG) is essential. Several factors, such as engine design and operating conditions, can affect the exhaust temperature, affecting the performance and efficiency of thermoelectric cells. Understanding these factors is essential for assessing the fuel-saving potential and emissions reduction through waste heat utilization. It is also necessary to consider the economic and environmental benefits of fuel savings and emissions reduction to fully comprehend the role of thermoelectric cells in energy generation and sustainability, as reported by Sahin et al., [1].

TECs and heat pipes have been used in tandem to produce energy for applications using engine exhaust gases. This entailed creating a proof-of-concept bench model for thermoelectric cell power generation using heat pipes and hot engine exhaust gases, (Orr et al.,) [2]. Waste-heat recovery (WHR) has become an essential method of saving energy and reducing emissions in the automobile industry. TEGs are a promising technology for producing electricity from low-level thermal energy. They are easy to operate, compact, have a long service life, and require low maintenance costs. Due to its environmental friendliness, thermoelectric devices are becoming increasingly popular as a flexible and green source of electricity. ICEs are extensively used in our daily lives for either gasoline or diesel engines. During light-duty applications, 40% of the thermal energy of combustion is wasted as exhaust gas, whereas two-thirds is lost as waste heat in automobiles, (Yu et al.,) [3]. The ICE energy path shown in

http://doi.org/10.30684/etj.2024.153438.1815
Received 08 September 2024; Received in revised form 12 October 2024; Accepted 19 October 2024; Available online 01 December 2024
2412-0758/University of Technology-Iraq, Baghdad, Iraq

Figure 1(a) indicates that approximately 25% of the fuel can be used to power vehicles. The TECG can transform this waste heat into electrical power. This electricity can be returned to an auxiliary or hybrid battery pack, as reported by Crane and Jackson [4]. Hence, the alternator can be operated at part load, which increases the efficiency of the vehicle and improves the fuel economy. Energy conversion from waste thermal energy to sound electrical energy is known as thermoelectric (TE) energy conversion, and it is thought to be one way to address the issues highlighted above [5-7]. TEGs in the WHR systems have numerous advantages over other waste heat recovery technologies, including small size, lack of moving parts, lack of chemical interactions, and low maintenance requirements. TEGs' poor efficiency compared to a Rankine cycle WHR system is a disadvantage, (Ringler et al.,) [8]. The modeling studies have been carried out to evaluate the performance of the TEG (Gou et al.,) [9].

Studying the influence of the transient behavior of TEG under various start-up modes on constant current voltage and power, it is discovered that there is a slight variation in temperature progression with various currents during startup procedures (Yu et al.,) [10]. Numerous studies have shown that the electricity generated by TEG can be used as a valuable power source for vehicles and can significantly increase the internal combustion engine's (ICE) efficiency and optimize the design parameters [10-14]. Hsiao et al. [15], produced a one-dimensional thermal resistance model to forecast TEG performance in the exhaust pipe and radiator positions, two possible locations in a car. The micro-channel heat sink was used to evaluate the geometrical impact of TECG on the characteristics of heat transfer, Wang et al. [16], Rezania et al., [17]. Other applications of TECG, created the prototype of a small-scale thermoelectric incinerator for environmentally friendly trash disposal and electricity production, good temperature distribution analyzed using computational fluid dynamics (CFD) models [18-22]. The thermal energy can be recovered to improve fuel consumption and system efficiency and reduce engine gas emissions [23,24]. The use of TECG for automobile IC engine heat recovery has been demonstrated by several papers that installed the devices in the vehicle exhaust [25-27]. TEC application uses two distinct heat sink types to examine the performance of solar-powered TEC refrigerator units with a 30-liter capacity for two scenarios presented in, Nora et al., [28]. Previous studies [29,30] show that TEG technology is an environmentally friendly vehicle. This work aims to assess the possibility of useful EPG for engine waste heat. It is essential to evaluate the TEG system used in ICE waste heat recovery under various fuel circumstances (gasoline and CNG) (Abdelghany et al.,) [31]. Numerous analytical and computational models have been investigated to gain a deeper understanding of the operation and performance of TEGs. For instance, a technique for modeling a low-temperature gradient TEG system with a workable power conversion stage was presented by [32,34]. Peiyong et al. [35], proposed the TEG device's power density, voltage, power, and conversion efficiency with engine loads and its heat, flow, and electrical field distributions for diesel engines.

Therefore, this experimental study aims to investigate the waste-heat recovery of IC engine exhaust systems and its effects on engine performance, such as BSFC and emissions; this field still requires ongoing investigation. The engine exhaust pipe is modified to install forty TECs, and the output EPG by forty TECs system is assessed for feeding electrical loads. The operation parameters such as exhaust temperature, exhaust gas flow rate, TEC's cold and hot surface temperature, and BSFC are evaluated at various engine speeds of 50 and 100 N.m. The rest of the present paper is organized as follows: TEG Theory and thermal behavior are presented in Section 2. An experimental apparatus and test procedure are described in Section 3. The results and discussion are analyzed in Section 4 and the conclusions.

2. TEG theory and thermal behavior

2.1 Brief history of thermo-electrics

Thermoelectricity was discovered and developed in Western Europe by academic scientists in the century preceding the world wars, with a large portion of the activity concentrated on Berlin. Thomas Johann Seebeck discovered 1821 that a compass magnet would be deflected by a circuit composed of two dissimilar metals with connections at different temperatures , (Seebeck) [36]. At first, Seebeck felt this might have something to do with the Earth's magnetic field and assumed it was caused by magnetism brought on by the temperature differential. It was soon discovered, nevertheless, that a "Thermoelectric Force" created an electrical current, which deflects the magnet according to Ampere's equation. More precisely, an electric current in a closed circuit can be driven by the electric potential (voltage) created by the temperature differential. This is now referred to as the Seebeck effect. Using the idea of the 'Figure of Merit' ZT, Abram Fedorovich Loffe created the contemporary theory of thermoelectricity in 1949. This work culminated in the seminal works on Semiconductor Thermo-elements and Thermoelectric Cooling by Vedernikov et al., [37]. Loffe also advocated using semiconductors in semiconductor physics and thermo-electrics for performance optimization and outcome analysis. The most well-known tellurides of antimony, bismuth, and lead are extensively doped semiconductors with high thermoelectric figures of merit. Some of the first commercial thermoelectric power production and cooling devices were developed due to Loffe and his institute in Saint Petersburg's vigorous pursuit of thermoelectric research and development in the USSR. Loffe was among the first to advocate for alloying to lower point defects' lattice thermal conductivity.

2.2 Thermoelectric industry

Numerous materials have been considered beneficial for producing thermoelectricity since Seebeck's discovery. Electric conductors and semiconductors, including antimony, bismuth, copper, iron, lead, zinc, and other alloys, were the foundation of the earliest TEGs1. Numerous other thermoelectric materials (TMs), such as composites and ceramics, were created later in the 20th Century. A tiny but steady industry was established to manufacture Peltier coolers based on Bi_2Te_3-Sb_2Te_3 and thermocouples. These coolers are currently used in various devices, including seat cooling/heating systems, small refrigerators, and optoelectronics. Some specialized uses for thermoelectric power generation are made possible by the demand for dependable, distant power sources. The process of using TEGs to harness the Seebeck Effect and transform a temperature differential into

electrical energy is known as thermal energy harvesting. The characteristics of a unique class of semiconductors called thermoelectric materials cause this phenomenon. An electric potential is produced when heat energy moves through them from a hotter side to a colder side (Alexandre et al.,) [38].

2.3 Seebeck effect

The TEC comprises two ceramic plates that form a foundation for n-type and p-type semiconductor thermo-elements materials, offering mechanical integrity and electrical insulation. The temperature differential, load resistance, and the characteristics of the semiconductor materials all affect the electrical power output. Utilizing TEC cells, thermal energy from the various temperature gradients between a semiconductor's hot and cold ends can be transformed into electrical energy, Equation (1) determines the thermoelectric material's figure-of-merit, Temizer et al., [4].

$$Z = \frac{a^2}{K\delta} \tag{1}$$

where a it is the Seebeck coefficient, δ is the electric resistivity, k is the total thermal conductivity, and Z is the thermoelectric material's figure-of-merit.

Figure 1(b) shows the energy conversion procedure of a TECG system. The TECG is effectively operated due to the changes in the internal quantum system of the TE material. To realize the practical importance as a generator in heat recovery units, it is necessary to increase the conversion efficiency of the TE material and to improve the heat transfer from the exhaust gas to the TEC, a thermoelectric module, p-type and n-type semiconductors are used instead of metal conductors, (Suter et al.,) [29].

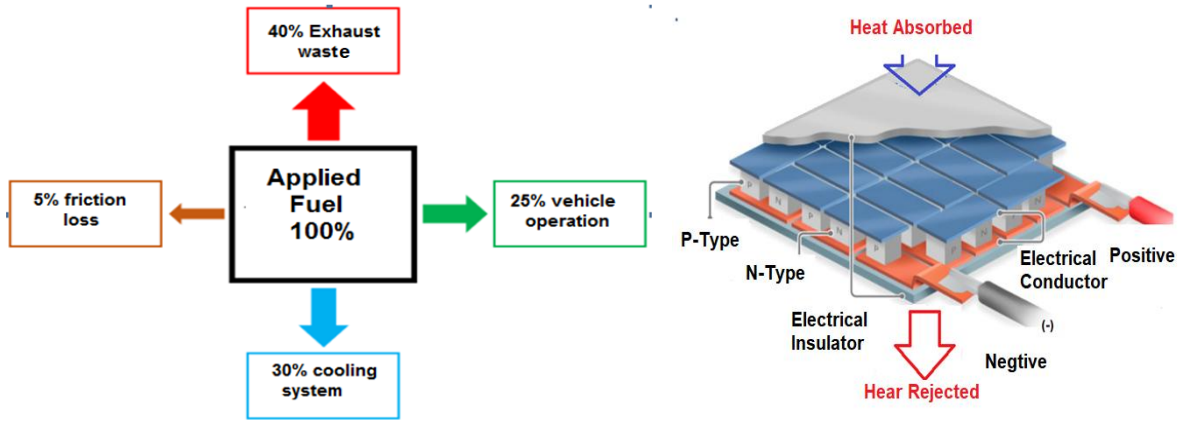

(a) The energy flow in ICE **(b) TEC structure**

Figure 1: (a) Typical energy flow path in ICE (b) Thermoelectric cell structure

The Seebeck effect converts a TD between two semiconductors into an electrical current. As shown in Figure 2(a), some free electrons and holes start to move, producing a current. The temperature differential between the two junctions causes a potential difference, or voltage, which is expressed by Equation (2):

$$V = a\Delta T = T_H - T_C \tag{2}$$

where ΔT is the TD between the two junction temperatures, V is the voltage of the TE, and T_H , T_C are the temperatures of the TE's hot and cold sides.

An ideal voltage source V and an internal resistance (R_{in}) make up the TEG's electrical equivalent circuit. When a load resistor (R_L) is connected across the TEG's output terminal, and there is a temperature differential between the TEG's surfaces, current flows through the load resistor or passes through it, and the TEG provides power (P_{max}). The temperature differential between the TEG's surfaces directly correlates with the amount of electricity the device generates.

$$P_{\max} = \frac{\Delta T^2 a^2}{4R_{in}} \tag{3}$$

The TEG's short-circuit current (I_o) and open-circuit voltage (V_O) also serve as practical expressions of the maximum power at any temperature differential.

$$P_{\max} = \frac{V_o I_o}{4} \tag{4}$$

2.4 Thermoelectric generators equations

TECG is a solid-state apparatus that directly converts the temperature differences or thermal energy into sufficient electricity. As shown in Figure 2(b), an electrical current can be created due to the connection of two dissimilar materials with the temperature difference. In this application, the heat capacity of exhaust gas Q_{ex} is used in the following formula to estimate the heat energy in the function of the temperatures:

$$Q_{ex} = \dot{m} C_p (T_{ex} - T_o) \tag{5}$$

where T_{ex} is the exhaust gas temperature, T_o is the ambient temperature, and the exhaust gas flow rate ($\dot{m}$) are the sum of the air flow and the fuel flow through the cylinder, or it is measured, and C_p is the heat capacity of the exhaust gas. The efficiency of thermoelectric elements in converting heat to electricity can be calculated using the following Equation(6):

$$\eta_{th} = \left[\frac{T_h - T_c}{T_c}\right]\left[\frac{(1+ZT)^{0.5} - 1}{(1+ZT)^{0.5} + (T_c / T_h)}\right] \tag{6}$$

where ZT is the figure of merit, and T is the average temperature between hot and cold surfaces of the TEG, $T = (T_c + T_h)/2$ (Patyk et al.,) [21]. The generated electrical power of TEC is calculated according to the relations (7,8):

$$W_e = Q_h - Q_c \tag{7}$$

$$P_o = W_e = V_o I_o \tag{8}$$

where $W_e = P_o$ is the generated power, η_{th} efficiency of thermoelectric elements, Q_h heat input, Q_c heat removal, and the output current and voltage I_O and V_o respectively.

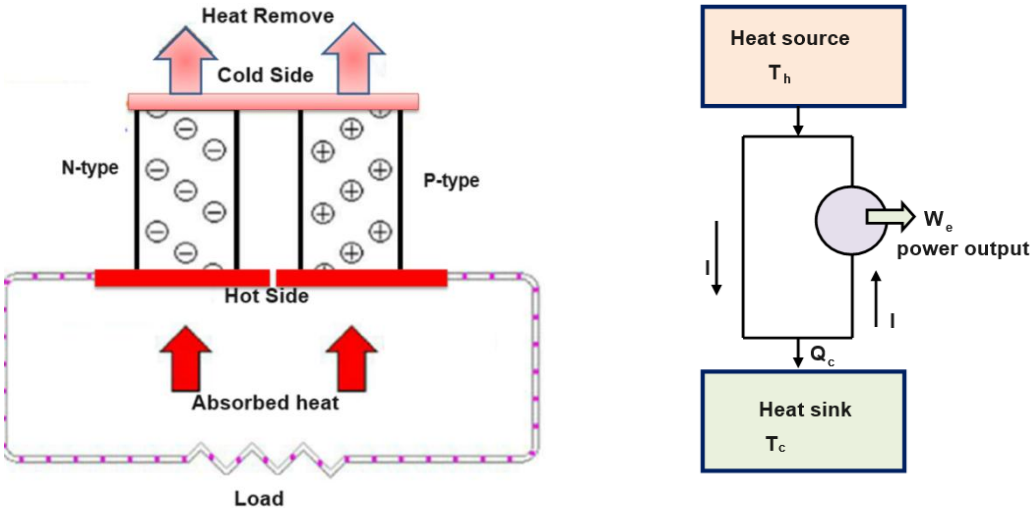

(a) Seebeck effect **(b) Electrical current**

Figure 2: Equivalent circuit of TEG: (a) Seebeck effect configuration (b) Electrical current configuration

The rate of heat supply at the hot side of thermocouples, for the Fourier effect, the rate of heat supplied Q_h by heat source and rate of heat removal Q_c by heat sink can be expressed as: (Temizer et al. [4], Abdelghany et al.) [31]:

$$Q_h = K_h (T_h - T_1) \quad and \quad Q_c = K_c (T_2 - T_c) \tag{9}$$

where K_h and K_c are the thermal conductivity of the hot side, and K_c is the thermal conductivity of the cold side, respectively. R_L is the total load resistance, T_1 is the temperature of the hot side of thermocouples, and T_2 is the temperature of the cold side of thermocouples. The output power of the parallel TEG is given by Equation (10):

$$P_o = I_o^2 R_L \tag{10}$$

The thermal efficiency of TEG is defined as the ratio between the power output and the heat input into the system. Equation (11) determines the thermal efficiency of TEG:

$$\eta_{th} = \frac{P_o}{Q_h} = \frac{I_o^2 R_L}{K_h (T_h - T_1)} \tag{11}$$

3. Experimental apparatus and test procedure

An experimental test rig stand is developed to evaluate the TECG's EPG output under different ICE exhaust muffler temperatures and the EPG-connected electrical load resistance. The system's effect on BSFC and engine emissions is also evaluated.

3.1 TEG and battery system preparation

Figure 3(a) shows the schematic supported and configuration of TECG in the engine exhaust system. With an external stainless steel sheet cover, the exhaust muffler has a rectangular shape. The dimensions of the muffler were 300 mm×180 mm × 60 mm. The TECs are supported between the muffler by steel wire and a cooling system to augment heat transport from the exhaust to the TECs' surface. The TECs are selected based on the temperature range characteristics. The specification parameters of the TEM cell (TEG1B-12610-5.1) modules used are tabulated in Table 1.

Figure 3(b) shows the settlements of the tests in the laboratory and connected the TECG in the engine exhaust system. On the upper and lower surfaces of the exhaust muffler, forty identical TEs were inserted to provide a heat source by allowing exhaust gas flow rate into the heat cooler through a bypass, (Patyk A et al.,) [21].

The 40 TECs were supported in four rows on the upper side in a (4 × 5) arrangement and four on the lower side in a (4 × 5) arrangement. The maximum electrical voltage can be calculated according to this relation. $V_{m,o} = 40n$, the maximum output current can be given by $I_{mo}=2m$, and the maximum output power of the TECG can be given by, $P_{m,o} = 7.1\ n\ m$. The heat energy of the TEC hot side and TECG efficiency can be calculated according to the relations (12 and 13):

$$Q_h = P_o + Q_{cw} \tag{12}$$

$$\eta_{TEG} = \frac{P_o}{Q_h} \tag{13}$$

During the experiment, a coolant pump (TDC-A12-0805) and valve assembly were used to maintain a steady coolant flow rate of 4 LPM in each coolant channel. The maximum flow rate of the coolant pump is 8 LPM, and the maximum power consumption is 17 W. The coolant was kept at a predetermined temperature of 30 ºC using a 20-L chiller. Before returning the heated coolant to the chiller, it was cooled principally via a plate-fin heat exchanger. Then, the output power is produced under the TD between the two sides of the modules and stored in load batteries from the rectifier. The net output power can be calculated according to the relations, $P_{net}=P_o - P_{pump}$, where P_{pump} is the power required of the electrical pump.

In an isolated charge system, batteries store excess energy that is converted into electrical energy. The overall system must be optimized in terms of available energy and local demand patterns. Li-ion batteries are used in the system for energy storage.

Table 1: TE power (TEG1B-12610-5.1) modules specifications

S/No.	Parameters	Values
1	Size	40 mm ×40 mm
2	Open circuit voltage	7.2 V
3	Internal resistance	1.8Ω
4	Match load output-voltage	3.6 V
5	Match load output-current	2 A
6	Match load output-power	7.2 W
7	Heat flux density	≃9.2 W/cm^2
8	Heat flux across the module	≃148 W
9	Hot side temperature	300 ℃
	Cold side temperature	30 ℃

3.2 Experimental set-up

The experimental setup is used for the Suzuki Swift gasoline engine considered in this work. The engine used in this study is a four-cylinder, four-stroke, water-cooled gasoline engine; the specification data of this gasoline engine is shown in Table 2. The TECG performance is evaluated using different engine operation conditions. The engine was coupled with an electrical dynamometer rated. The layout of the experimental setup is shown in Figure 4. The engine dynamometer was connected with a reaction torque transducer (Lebow model 2404-5k). The engine dynamometer is 90 kW, 160 N.m, and 6500 rpm. The system temperatures are measured by K-type thermocouples, such as the exhaust gas temperature,TEC's hot and cold surface temperature, and ambient air temperature. The voltage and current of TECG are measured using a model PA2200 analyzer. The engine control unit (ECU) is used to measure BSFC. The concentrations of exhaust THC (ppm), NO_x (ppm), CO (vol%), and CO_2 (vol%) were measured using a HOMANS gas analyzer. The gas analyzer specifications and accuracy details are presented in Mohamed [30].

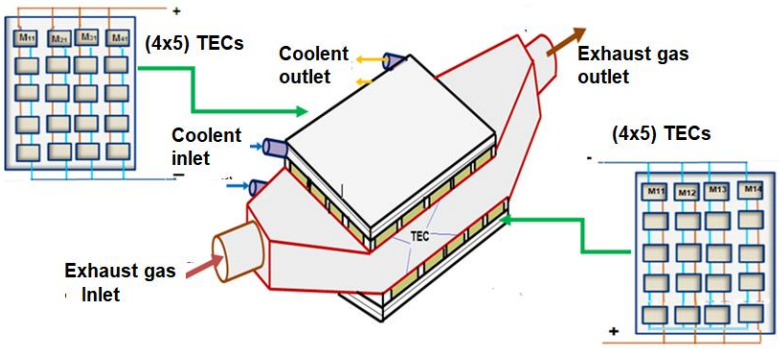

(a) Structure of TEC segments in muffler

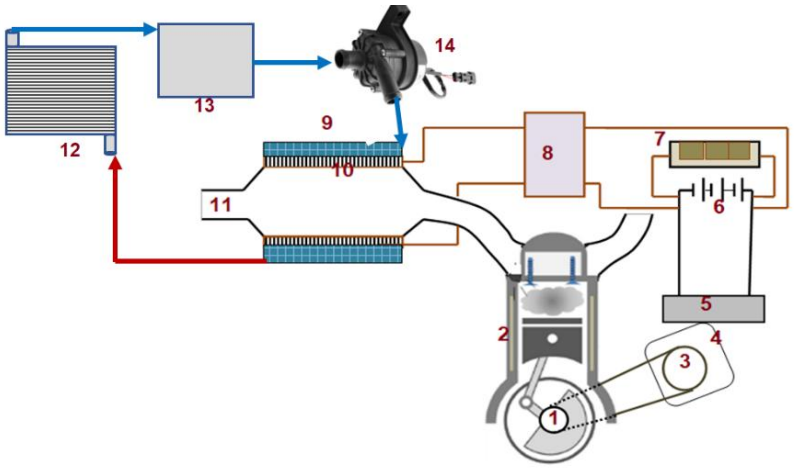

1. Crank engine pulley
2. IC Engine
3. Alternator pulley
4. Alternator
5. Rectifier
6. Battery
7. Electrical load
8. PUC
9. TEMs
10. Exhaust system
11. Exhaust output
12. Heat exchanger
13. Chiller
14. pump

(b) Schematic diagram of the TEG system

Figure 3: (a) Structure of TEC segments in muffler (b) Schematic diagram of TEC system

3.3 Experimental procedure

The engine was run in a steady state with WOT, with a variable engine speed from 1500 rpm to 4500 rpm and constant two engine loads of 50 N.m and 100 N.m, in accordance with the SAE J1349 testing protocol. The exhaust temperature was measured, and the exhaust emissions, BSFC, and EPG were evaluated with and without TECG. The flowchart in Figure 5 presents the experimental procedure.

Table 2: A Suzuki swift engine specification

No.	Parameters	Values
1	Cylinder array	In line 4 cylinder
2	Swept volume	1197 cm^3
3	valves per cylinder	Four
4	Compression ratio	11:1
5	Maximum power	83 BHP @ 5500 RPM
6	Maximum torque	115 Nm @ 3500 RPM
7	Cylinder bore	73 mm
8	Valve per cylinder	4
9	Firing order	1-3-4-2

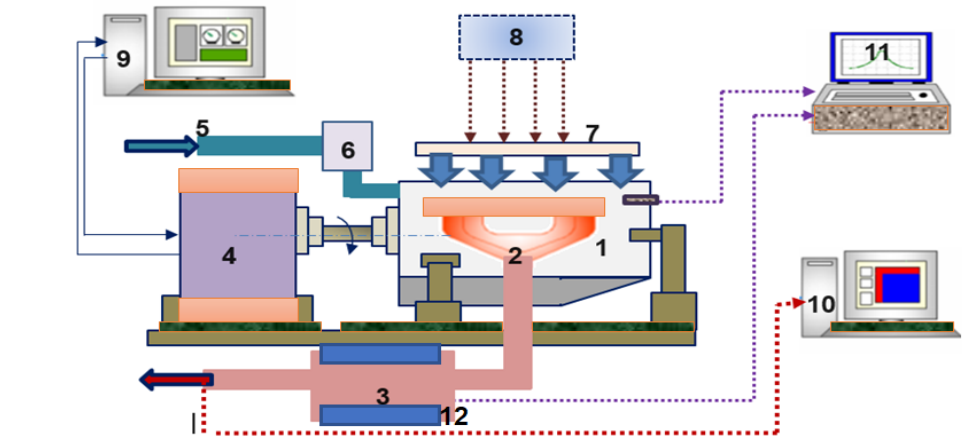

Figure 4: Schematic diagram of experimental system and measurement system

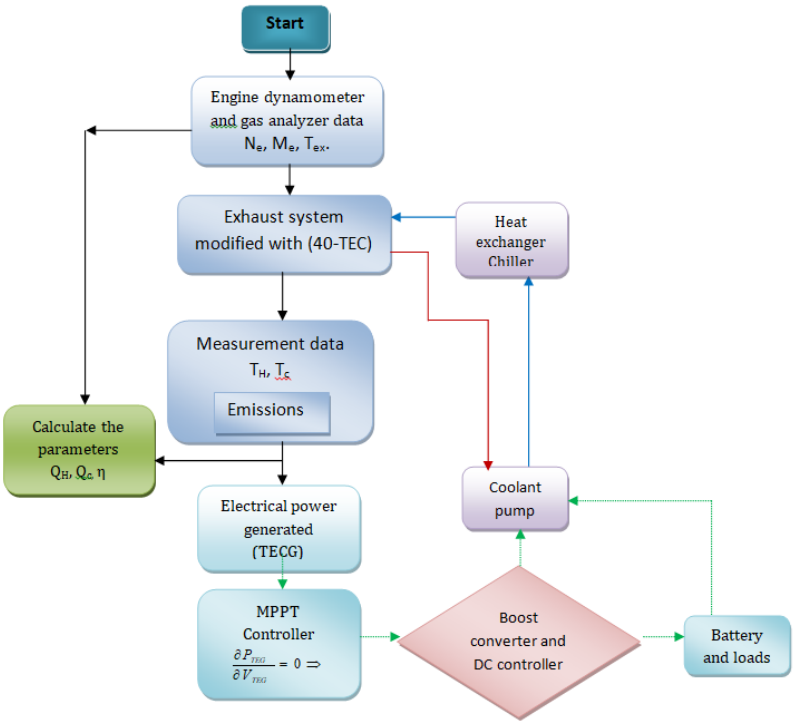

Figure 5: Flow chart of the experimental procedure steps

4. Results and discussion

The effect of engine exhaust temperature on TECG output power generation has been evaluated. The experimental result settings were as follows:

1) Exhaust temperature, BSFC, exhaust gas flow rate, and emissions characteristics behavior of the IC engine are evaluated through various engine speeds and two different engine loads 50 and 100 N.m inactive TECG
2) The performance of the TECG output power was assessed with two engine loads, 50 and 100 N.m, and at various engine speeds
3) A comparative study of an engine BSFC and emissions with active and inactive TECG systems

4.1 Exhaust temperature, BSFC, and emissions behavior of the IC engine

The evaluation of engine exhaust temperature is crucial for successfully implementing thermoelectric cells for EPG. This section presents the exhaust temperature, gas flow rate, BSFC, and emission behavior under inactive TECG. The engine warmed up at coolant temperature at T_C = 90 ℃ and stability in output power. The experimental procedure carried out the engine parameters without the supported TECG system in the exhaust muffler. Figure 6(a) illustrates the impact of engine speed on

exhaust temperatures by considering two load conditions: the exhaust temperature increases during engine high speed. An engine's maximum exhaust temperature values for 50 and 100 N.m loads are 335 ℃ and 387 ℃ at 4500 rpm, respectively. Figure 6(b) depicts the average exhaust temperatures with different engine speeds and loads. The average exhaust temperature was around 271 ℃ and 305 ℃ at 50 and 100 N.m loads, respectively. Figure 7(a) shows the exhaust flow rate during engine speeds and load. The engine exhaust flow rate increases at high speed. It was revealed that an engine's maximum exhaust flow rate loads 50 and 100 N.m is 60.45 g/s at 4500 rpm and 64.84 g/s at 4500 rpm, respectively. Figure 7(b) shows the BSFC with different engine speeds at 50 and 100 N.m loads; it is found that the BSFC values increased with the increase of high engine loads. According to earlier studies, these findings are consistent [22,31].

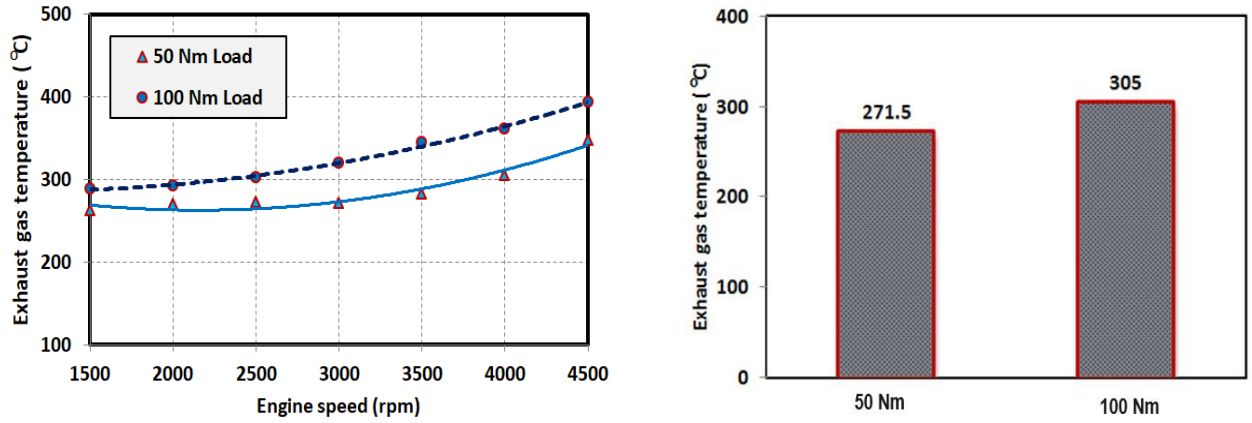

(a) (b)

Figure 6: (a) The exhaust temperature (b) Average values function of engine speeds

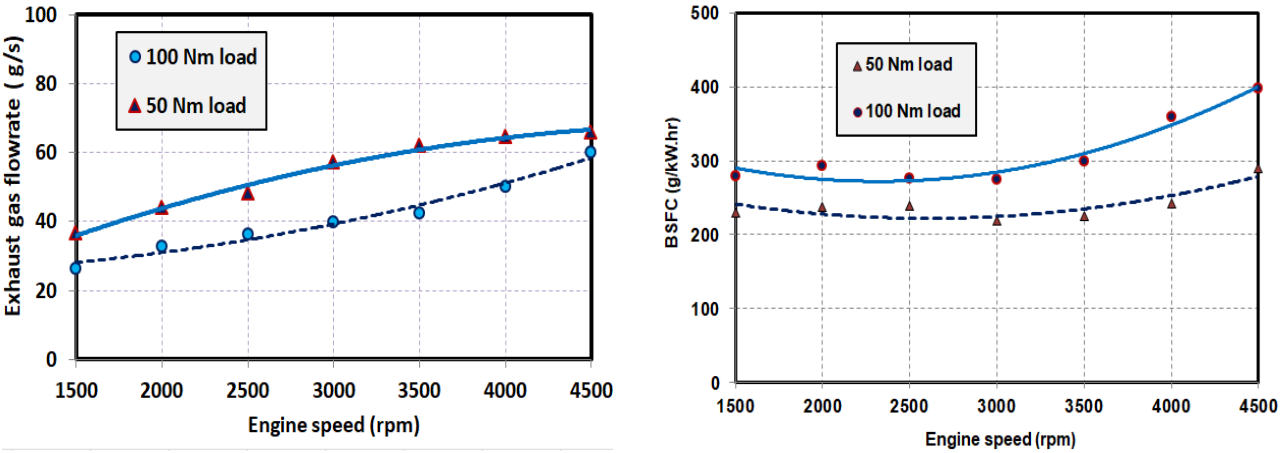

(a) (b)

Figure 7: (a) Exhaust gases flow rate (b) BSFC with different engine speeds

Figure 8 shows the exhaust emissions comparison with the variable speed from 1500 rpm to 4500 rpm and two load conditions. Figure 8(a) depicts the total hydrocarbon (THC) emissions at a variable speed; the THC emission decreases at high speed. The peak of THC concentration in the exhaust gas emission with engine loads at 50 N.m and 100 N.m is 1038.4 (ppm) and 661.7 (ppm) at a speed of 1500 rpm, respectively. Figure 8(b) illustrates the Nitrogen oxide (NO_x) emissions over a speed range; the NO_x emissions increase under high speed and high loads. The maximum value of NO_x concentration in the exhaust gas emission with engine loads at 50 N.m and 100 N.m is 872.7 (ppm) and 1425.6 (ppm) at a speed of 4500 rpm, respectively. Figure 8(c) illustrates the Carbon monoxide (CO) emissions over a speed range. The maximum value of CO concentration in the exhaust emission with engine loads at 50 N.m and 100 N.m is 5.62 (vol%) and 2.98 (vol%), respectively. Figure 8(d) shows that Carbon dioxide (CO_2) emission at the speed range, the CO_2 emissions increases with high loads and maximum value at 3500 rpm.

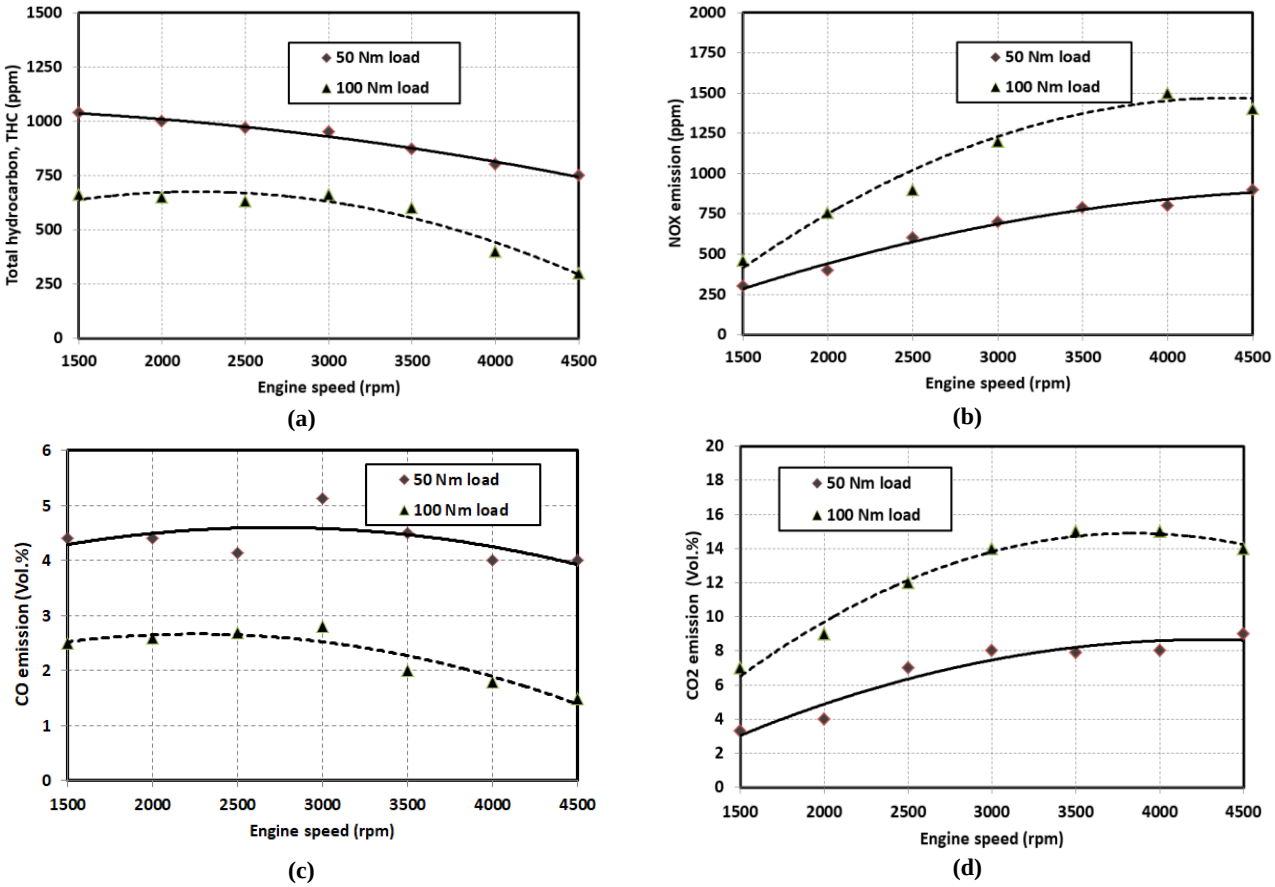

Figure 8: Exhaust emissions: (a) THC, (b) NO_x, (c) CO_2, (d) CO as a function of the speeds

4.2 The temperature behavior and performance of TECG

The evaluation of TEC surface temperature is crucial for implementing EPG. This section presents the effect of the engine exhaust manifold on the TECG; Figure 9(a) presents the TEC surface temperature under different engine speeds and two load conditions. The hot and cold surface temperature increases with engine speed increase, increasing 100 N.m condition. The maximum hot surface side temperature of TECG for 50 and 100 N.m loads was 265 ^oC at 4500 rpm and 315 ^oC at 4500 rpm, respectively. And it was also found that the maximum cold surface side temperature of TECG for 50 and 100 N.m loads is 98.5 ^oC at 4500 rpm and 118.7 ^oC at 4500 rpm, respectively. The TEC operation is based on the different temperatures on the hot side and cold side. Figure 9(b) shows the different temperatures between the hot and cold sides at two load conditions. The maximum different temperature of TECG at 50 and 100 N.m loads is 157.8 ^oC at 4500 rpm and 192.5 ^oC at 4500 rpm, respectively. The TD is the main factor in the production of TECG.

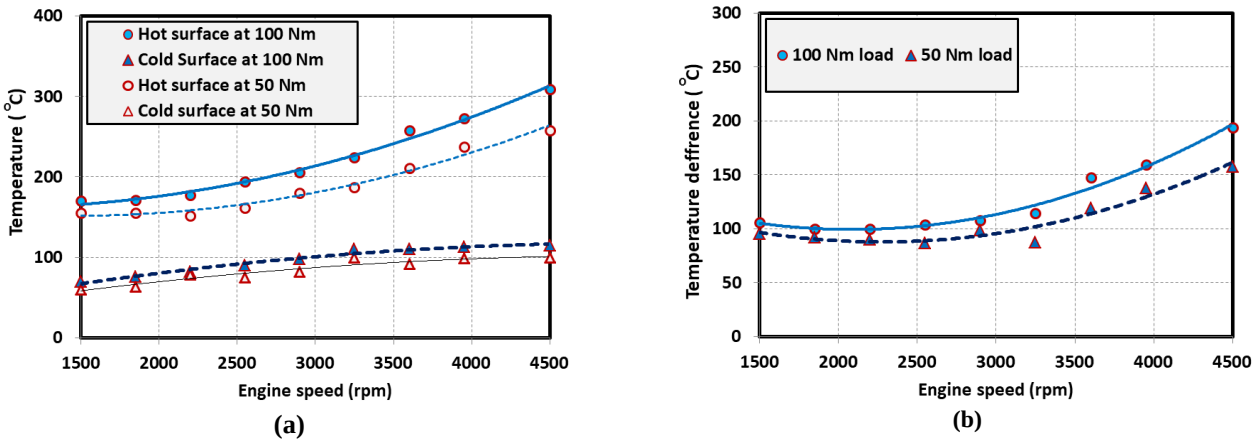

Figure 9: (a) The surface temperatures difference between cold and hot surfaces of TEC, (b) Temperatures difference with loads

From maximum power point tracking (TMPP) of the TECG output power, a power conditioning unit (PCU) must be configured with a battery voltage of 14.5 V. The electric power generated from the active TECG was fed to the engine electrical system by connecting the output of PCU to power all electrical loads of the engine. Figure 10(a) depicts the TECG voltage with

current with different speeds at 50 N.m load, and Figure 10(b) depicts the TECG voltage with different speeds at 100 N.m load. The I-V curves exhibit an almost linear trend regardless of engine load and rotation speed, indicating a nearly constant electrical resistance throughout the experiment.

Figure 11(a) presents the TECG power output with load resistance at different speeds at 50 N.m load; it was also found that TECG power output increases under high speed. The maximum peak of the power generation by TEC is 185.8 W at a speed of 4500 rpm. Figure 11(b) shows the TECG power output with the load resistance at different speeds at 100 N.m load; the TEC power output increases under high speed, and it was also found that a maximum of EPG by TECG is 218.5 W at speed 4500rpm. The TECG yields the maximum EPG between 3 and 7 Ω load resistance (R_{load}). Figure 12(a) depicts TECG power output with the current under different speeds at 50 N.m and 100 N.m loads and 10 Ω load resistance; the peak of EPG output value is increased as the speed increased from 41.6 W to 68.2 W, 80.5 W, 118.8 W, and 136.7 W when the engine speed from 1500 rpm to 4500 rpm respectively at 50 N.m. Similarly, as shown in Figure 12(b), the peak of the EPG output value is increased as the speed increased from 68.2 W to 99.8 W, 142.6 W, 178.8 W, and 218 W when the engine speed from 1500 rpm to 4500 rpm respectively at 100 N.m. Based on improved temperature distribution at high engine load and speed, the results showed that TECG has sound EPG output.

Figure 13(a) depicts the TEG efficiency under different speeds at 50 N.m and 100 N.m loads. It was also found that the maximum efficiency of the TECG for 50 and 100 N.m loads is 10.8% and 12.4% at 4500 rpm, respectively. Figure 13(b) depicts the TEG's net output power with pump flow rate. The maximum TECG net power for 50 and 100 N.m loads is 142.5 W% and 182 W at 4500 rpm, respectively.

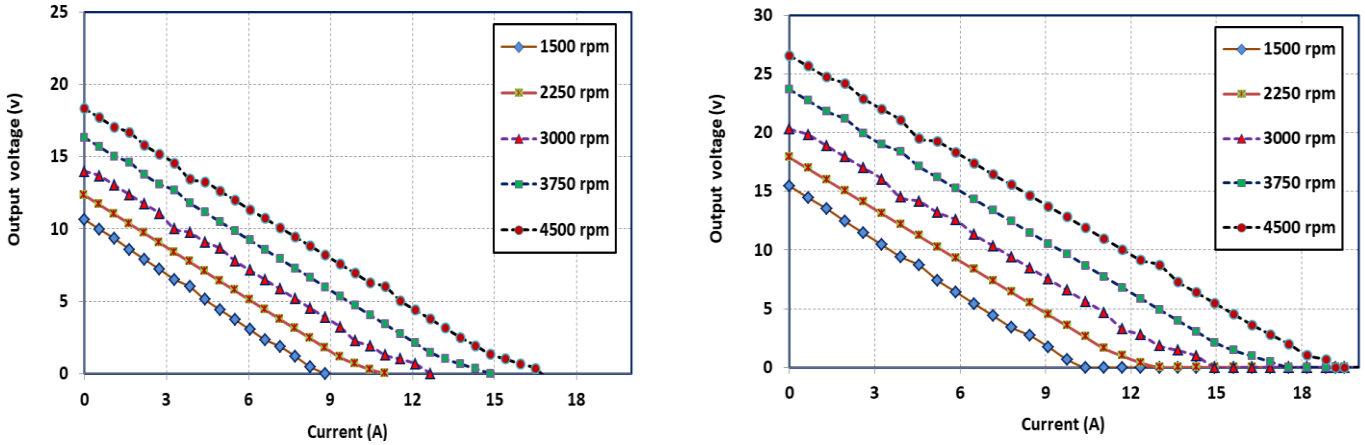

Figure 10: The TECG output voltage with the current: (a) 50 N.m load, (b) 100 N.m load

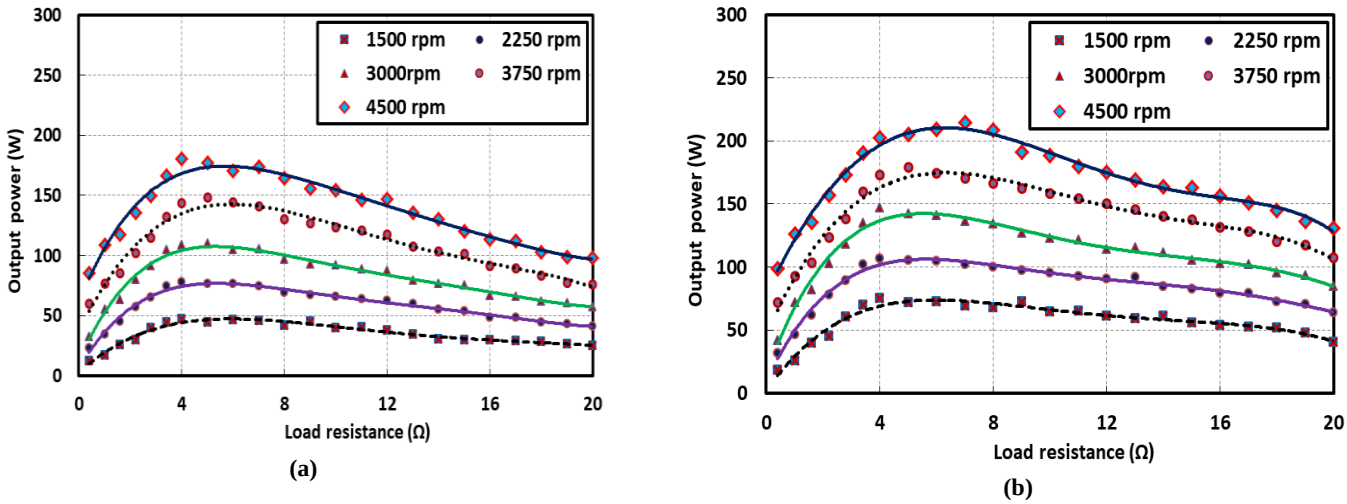

Figure 11: Power output of the TECG with the load resistance: (a) 50 N.m load, (b) 100 N.m load

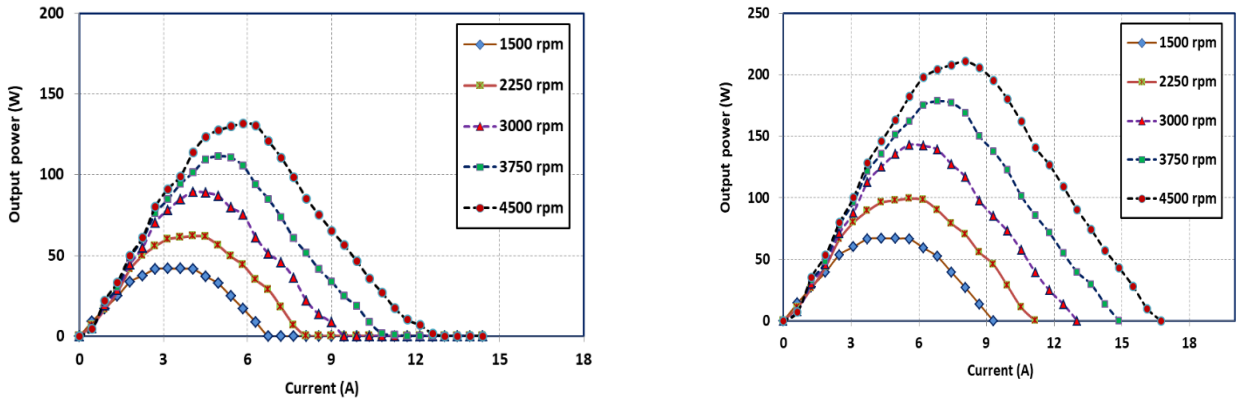

Figure 12: Power output of the TECG with the output current: (a) 50 N.m load, (b) 100 N.m load

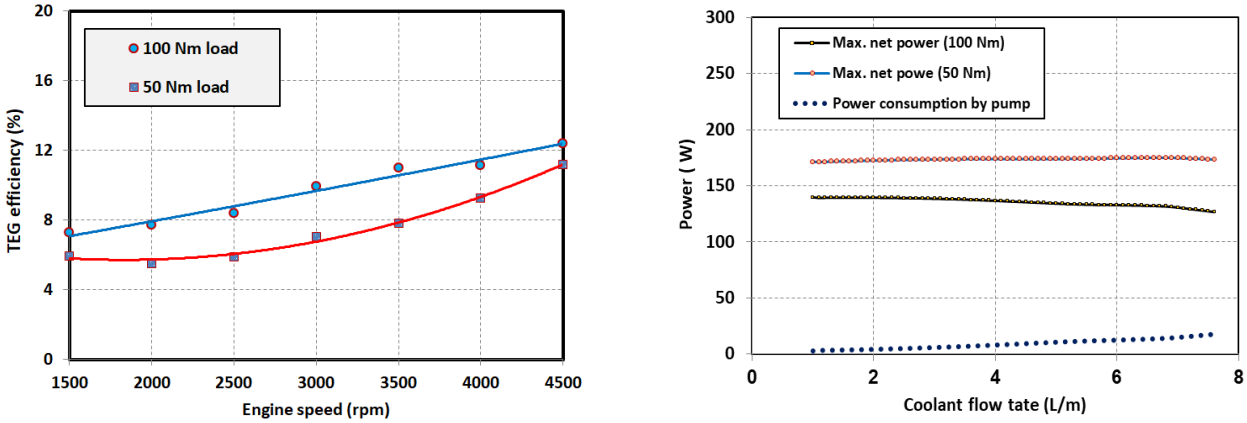

Figure 13: (a) TEG efficiency, (b) The net output power

4.3 Effect of the TECG system on BSFC and emissions

The engine ran steadily after the warm-up, with constant load at 50 N.m and 100 N.m at different speeds. Figure 14 (a) compares BSFC over a speed range and two load conditions with active and inactive TECG. A BSFC maximum value with inactive TECG for 50 and 100 N.m loads was 285.6 g/kw.hr at 4500 rpm and 393.7 g /kw.hr at 4500 rpm respectively. Also, it is found that the maximum value of BSFC with active TECG for 50 and 100 N.m loads is 251.3 g/kw.hr at 4500 rpm and 352.4 g/kw.hr at 4500 rpm respectively. Figure 14 (b) depicts the average values of BSFC at active and inactive TECG with two load conditions. The average values of BSFC at active TECG are found to be lower than inactive TECG with speed range and on an average of 2.89% and 2.56% lower than inactive TECG while the engine loads 50 N.m and 100 N.m, respectively.

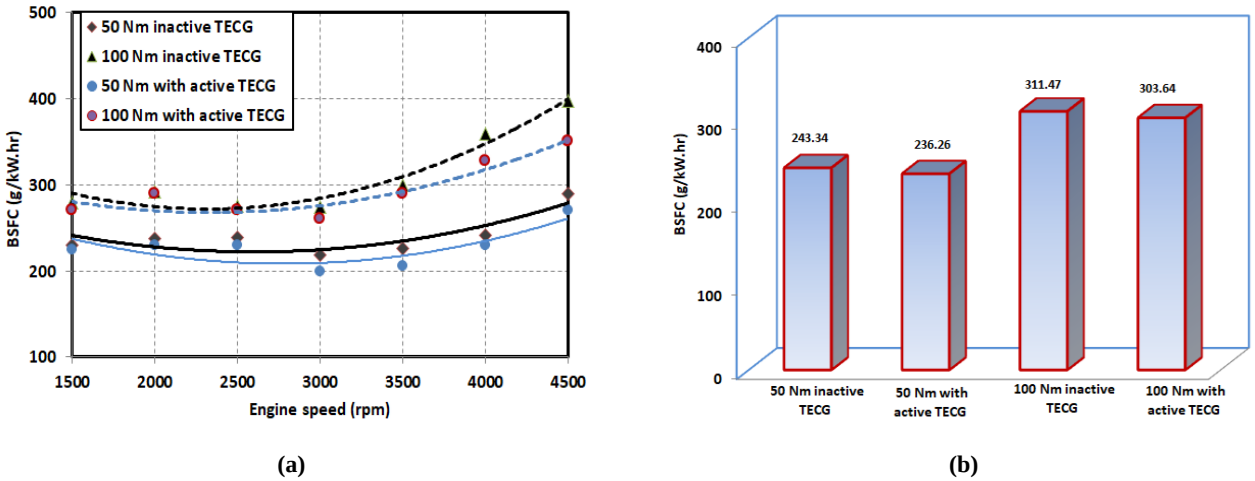

Figure 14: (a) BSFC over a speed range with active and inactive TECG (b) The average values of BSFC

Figure 15(a) shows the THC emission comparison with the variable speed from 1500 rpm to 4500 rpm under active and inactive TECG; the THC emissions decrease under high speed for all cases. The highest possible quantity of THC in exhaust gas emissions with engine loads at 50 N.m and 100 N.m under inactive TECG is 1038.4 (ppm) and 661.7 (ppm), respectively. Also, it is found that the maximum value of THC at engine loads at 50 N.m and 100 N.m with active TECG is 893.7 (ppm) and 591.2 (ppm), respectively. Figure 15(b) depicts the average values of THC at active and inactive TECG with 50 N.m and 100 N.m loads. The average values of THC at active TECG are found to be lower than inactive TECG with speed range and on an average of 2.47% and 2.88% lower than inactive TECG while the engine loads 50 N.m and 100 N.m, respectively.

Figure 16(a) illustrates the NO_x emissions over a speed range for active and inactive TECG; the NO_x emissions increase under high speed and high loads. The maximum value of NO_x concentration in the exhaust gas emission with engine loads at 50 N.m and 100 N.m under inactive TECG is 1425.6 (ppm) and 872.7 (ppm), respectively. Also, it was found that the maximum value of NO_x at engine loads at 50 N.m and 100 N.m with active TECG is 1208.9 (ppm) and 766.5 (ppm), respectively. Figure 16(b) depicts the average values of NO_x at active and inactive TECG. The average values of NO_x at active TECG are found to be lower than inactive TECG with speed range and on an average of 4.71% and 6.42% lower than inactive TECG during the engine loads 50 N.m and 100 N.m, respectively. The results indicate that the active TECG significantly affects the NO_x emission.

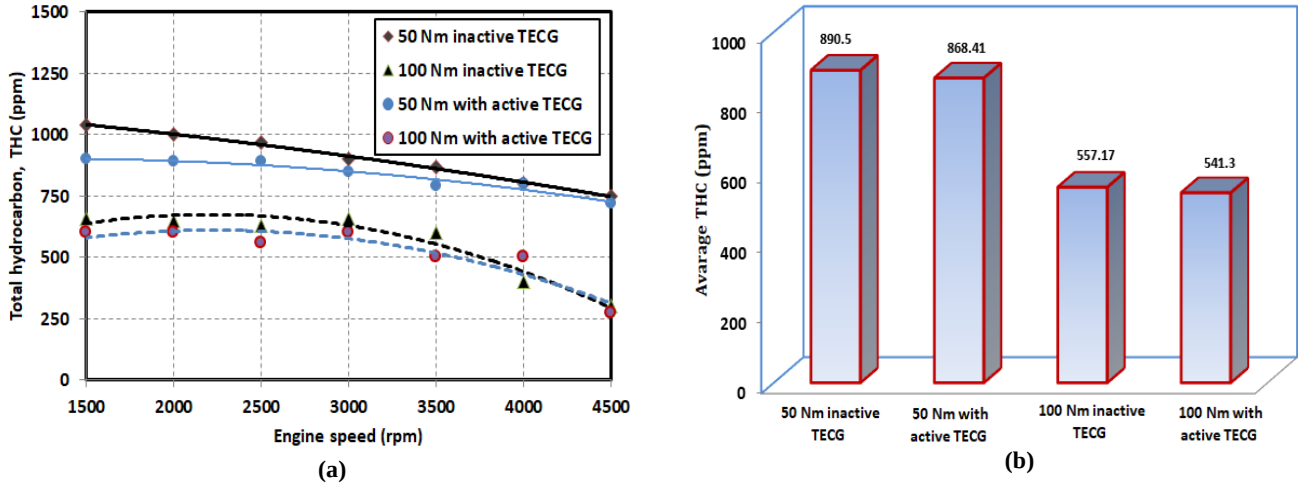

Figure 15: (a) THC emissions for active and inactive TECG (b) The average values of THC

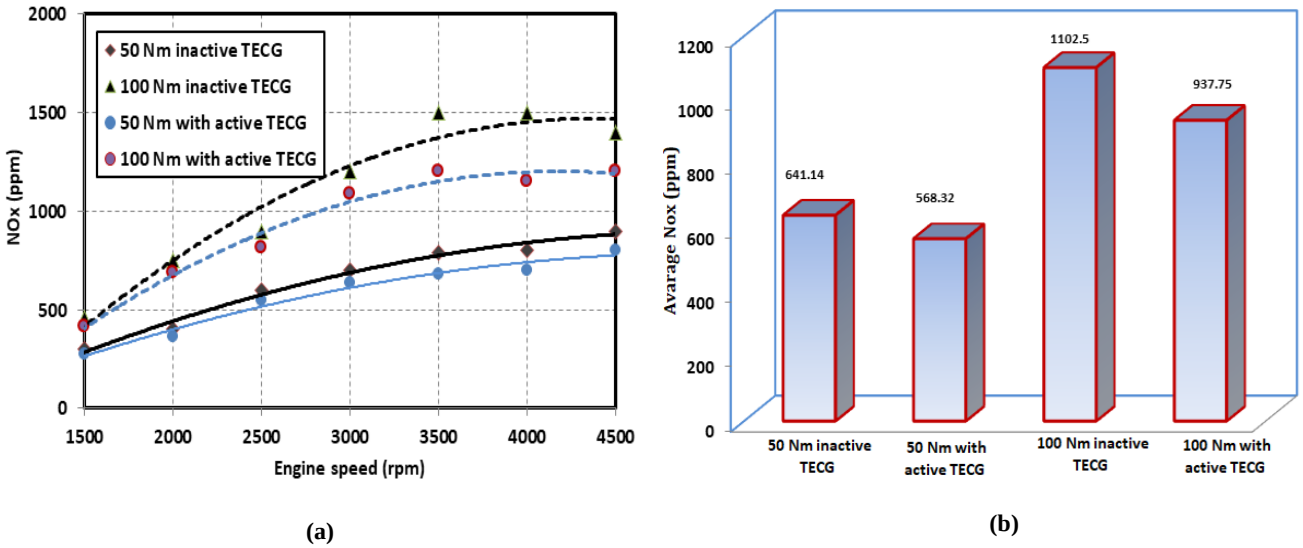

Figure 16: (a) NO_x emissions for active and inactive TECG, (b) The average values of NO_x

Figure 17(a) illustrates the CO emissions over a speed range for active and inactive TECG. The maximum value of CO concentration in the exhaust gas emission with engine loads at 50 N.m and 100 N.m under inactive TECG is 5.62 (vol.%) and 2.98 (vol.%), respectively, also show that the maximum value of CO concentration at engine loads at the 50 N.m and 100 N.m with active TECG is 4.23 (vol.%) and 2.92 (vol.%) respectively. Figure 17(b) depicts the average values of CO at active and inactive TECG. The average values of CO at active TECG are found to be lower than inactive TECG with speed range and on an average of 1.92% and 5.12% lower than inactive TECG while the engine loads 50 N.m and 100 N.m, respectively. Figure 18(a) shows that CO_2 emissions are over the speed range, and the CO_2 emissions increase with high speed and high loads-the average values of CO_2 at active and inactive TECG, as shown in Figure 18(b). The average values of CO_2 at active TECG are found to be lower than inactive TECG with speed range and on an average of 4.32% and 4.52% lower than inactive TECG while the engine loads 50 N.m and 100 N.m, respectively.

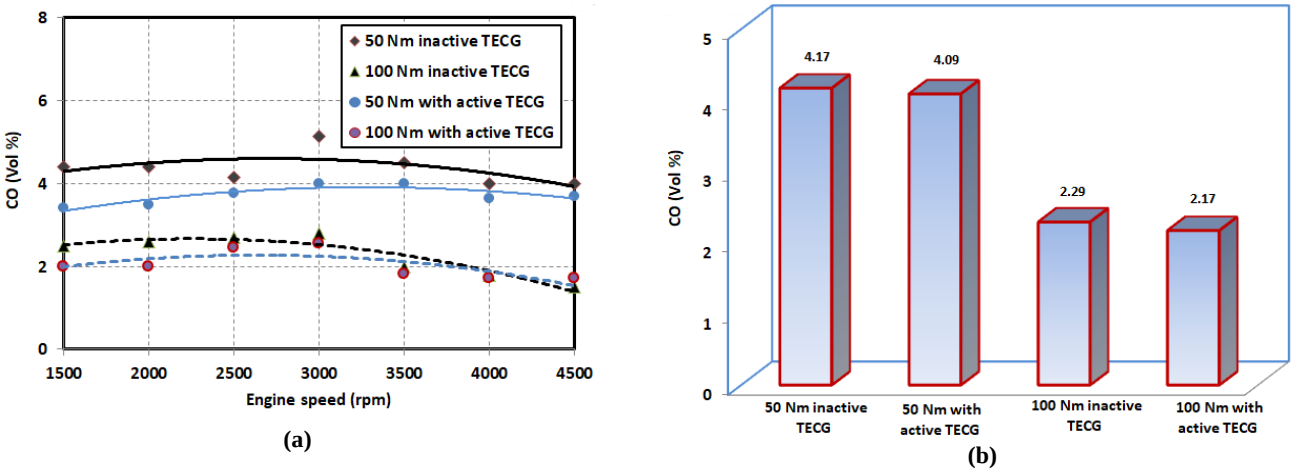

(a) **(b)**

Figure 17: (a) CO emissions for active and inactive TECG (b) The average values of CO

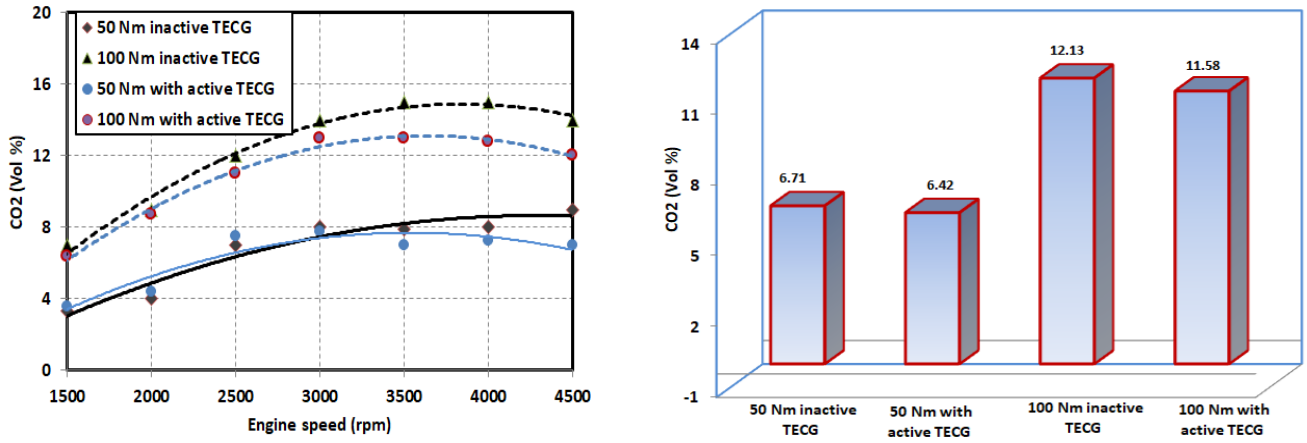

(a) **(b)**

Figure 18: (a) CO_2 emissions for active and inactive TECG (b) The average values of CO_2

5. Conclusion

The primary results of the current study, which involved a TECG performance experiment with 40 TECs using EHR for gasoline engines, are as follows:

1) Forty TEC units (TEG1B-12610-5.1) are supported to the exhaust line of the Suzuki Swift gasoline engine to heat supply. The experimental equipment used in this work could be used to assess the exhaust flow rate, exhaust temperatures, BSFC, and emission characteristics. The TECG output power performance is evaluated. A comparative study of an engine BSFC and emissions with an active and inactive TECG system is conducted.
2) The temperatures of exhaust gas increase with the increase of engine load and speed. The maximum values of an engine exhaust temperature for 50 and 100 N.m loads are 335 ℃ and 387 ℃ at 4500 rpm, respectively. The average exhaust temperature was around 271 ℃ and 305 ℃ at 50 and 100 N.m loads, respectively.
3) The maximum EPG by the TECG system at 50 and 100 N.m engine loads are 185.8 w and 218.5 w at an engine speed of 4500 rpm, respectively. The results indicate that the proposed TECG system, supported by a gasoline engine, is effective at high speed and load.
4) The average value of BSFC with active TECG is lower than that of the inactive TECG and on an average of 2.89% and 2.56% lower than inactive TECG during the engine loads 50 N.m and 100 N.m, respectively.
5) The results indicate that an average value of engine emissions such as THC, NO_x, CO, and CO_2 with active TECG is lower than that of an inactive TECG throughout the speed range and two engine loads. The average values of THC at active TECG are found to be lower than inactive TECG with speed range and on an average of 2.47% and 2.88% lower than inactive TECG while the engine loads 50 N.m and 100 N.m, respectively. The results obtained indicate that the active TECG significantly affects the NO_x emission.
6) The average values of CO at active TECG are found to be lower than inactive TECG with speed range and on an average of 1.92% and 5.12% lower than inactive TECG during the engine loads 50 N.m and 100 N.m, respectively. The average values of CO_2 at active TECG are found to be lower than inactive TECG; the average values of CO_2 are 4.32% and 4.52% lower than inactive TECG throughout the speed range and two engine loads.

Abbreviations

ADC Analog-to-digital converter

BSFC	Brake specific fuel consumption
DAQ	Data acquisition system
ECU	Engine control unit
EGHR	Exhaust gas heat recovery
EPG	Electrical power generated
GFC	Gasoline fuel consumption
ICE	Internal combustion engine
MPPT	Maximum power point tracking
PCU	Power conditioning unit
PWM	Pulse-width-modulated
SAE	Society of Automotive Engineering
TD	Temperature difference
TE	Thermoelectric
TECG	Thermoelectric cell generators
TEMs	Thermoelectric modules
WHR	Waste-heat recovery
WOT	Wide open throttling

Funding

This research received no specific grant from any funding agency in the public, commercial, or not-for-profit sectors.

Data availability statement

The data that support the findings of this study are available on request from the corresponding author.

Conflicts of interest

The authors declare that there is no conflict of interest.

References

[1] A. Z. Sahin, B. S. Yilbas, S. Z. Shuja, O. Momin, Investigation into topping cycle: Thermal efficiency with and without the presence of thermoelectric generator, Energy, 36 (2011) 4048 - 4054. https://doi.org/10.1016/j.energy.2011.04.044

[2] B. Orr, B. Singh, L. Tan, A. Akbarzadeh, Electricity generation from an exhaust heat recovery system utilizing thermoelectric cells and heat pipes, Appl. Therm. Eng., 73 (2014) 588-597. https://doi.org/10.1016/j.applthermaleng.2014.07.056

[3] C.Yu, K.T. Chau, Thermoelectric automotive waste heat energy recovery using maximum power point tracking, Energy Convers. Manag., 50 (2009) 1506–1512. https://doi.org/10.1016/j.enconman.2009.02.015

[4] D. T. Crane, G. S. Jackson, Optimization of cross flow heat exchangers for thermoelectric waste heat recovery, Energy Conv. Manag., 45 (2003)1565-1582. https://doi.org/10.1016/j.enconman.2003.09.003

[5] I. Temizer, C. Ilkılıç, The performance and analysis of the thermoelectric generator system used in diesel engines, Renew. Sustain. Energy, Rev., 63 (2016) 141–51. https://doi.org/10.1016/j.rser.2016.04.068

[6] J. Merkisz, P. Fuc, P. Lijewski, A . Ziolkowski, M .Galant, M. Siedlecki, Analysis of an increase in the efficiency of a spark ignition engine through the application of an automotive thermoelectric generator, J. Electron. Mater., 45 (2016) 4028 - 4037. https://doi.org/10.1007/s11664-016-4543-0

[7] X. Liu, Y.D. Deng, Z. Li, C.Q. Su, Performance analysis of a waste heat recovery thermoelectric generation system for automotive application, Energy Convers. Manage., 90 (2015) 121-127. https://doi.org/10.1016/j.enconman.2014.11.015

[8] G. Liang, J . Zhou, X . Huang, Analytical model of parallel thermoelectric generator, Appl. Energy, 88 (2011) 5193-5199. https://doi.org/10.1016/j.apenergy.2011.07.041

[9] J. Ringler, M. Seifert, V. Guyotot, W. Hübner, Rankine cycle for waste heat recovery of IC Engines, SAE Int. J. Engines., 2 (2009) 67-76. https://www.jstor.org/stable/26308377

[10] X. Gou, S. Yang, H. Xiao, Q. Ou, A dynamic model for thermoelectric generator applied in waste heat recovery, Energy 52 (2013) 201- 209. https://doi.org/10.1016/j.energy.2013.01.040

[11] S. Yu, Q. Du, H. Diao, G. Shu, G. Jiao, Start-up modes of thermoelectric generator based on vehicle exhaust waste heat recovery, Appl. Energy, 138 (2015) 276–290. https://doi.org/10.1016/j.apenergy.2014.10.062

[12] JH. Meng, XX. Zhang , XD. Wang, Dynamic response characteristics of thermoelectric generator predicted by a three-dimensional heat-electricity coupled model, J. Power Sources, 245 (2014) 262-269. https://doi.org/10.1016/j.jpowsour.2013.06.127

[13] X. Gou, H. Xiao, S.Yang, Modeling, experimental study and optimization on low temperature waste heat thermoelectric generator system, Appl. Energy, 87 (2010) 3131-3136. https://doi.org/10.1016/j.apenergy.2010.02.013

[14] X. Liang, X. Sun, H. Tian, G. Shu, Y. Wang, X. Wang, Comparison and parameter optimization of a two-stage thermoelectric generator using high temperature exhaust of internal combustion engine, Appl. Energy, 130 (2014) 190-199. https://doi.org/10.1016/j.apenergy.2014.05.048

[15] E. S. Mohamed, Development and performance analysis of a TEG system using exhaust recovery for a light diesel vehicle with assessment of fuel economy and emissions, Appl. Thermal Eng., 147 (2019) 661-674. https://doi.org/10.1016/j.applthermaleng.2018.10.100

[16] Y. Y. Hsiao, W. C.Chang, S. L.Chen, A mathematic model of thermoelectric module with applications on waste heat recovery from automobile engine, Energy, 35 (2010) 1447- 1454. https://doi.org/10.1016/j.energy.2009.11.030

[17] XD. Wang, YX. Huang, CH. Cheng, DW. Lin, CH. Kang , A three-dimensional numerical modeling of thermoelectric device with consideration of coupling of temperature field and electric potential field, Energy, 47 (2012) 488- 497. https://doi.org/10.1016/j.energy.2012.09.019

[18] A. Rezania, L. A. Rosendahl, Thermal effect of a thermoelectric generator on parallel microchannel heat sink, Energy, 37 (2012) 220-227. https://doi.org/10.1016/j.energy.2011.11.043

[19] Y. K. Sofi, R. H. Hendaryati, A. Rahmandhika, R. Hidayatulloh, M. F. Budiman, G.W. As'adi, R. Zaroby, W. S. Nugroho, Small-Scale thermoelectric incinerator prototype for sustainable waste management and power generation, Eng. Technol. J., 42 (2024) 986 -1000. https://www.iasj.net/iasj/article/320011

[20] K. Hanamura,T. Kumano,Y. Iida, Electric power generation by super-adiabatic combustion in thermoelectric porous element, Energy, 30 (2005) 347-357. https://doi.org/10.1016/j.energy.2004.05.010

[21] J. Martins, L. Goncalves, J. Antunes, F. Brito,Thermoelectric exhaust energy recovery with temperature control through heat pipes, SAE Int. J. Engines, 2011(2011) 1-19. http://dx.doi.org/10.4271/2011-01-0315

[22] A. Patyk, Thermoelectric generators for efficiency improvement of power generation by motor generators environmental and economic perspectives, Appli. Energy, 102 (2013) 1448-1457. https://doi.org/10.1016/j.apenergy.2012.09.007

[23] M. Lossec, B. Multon, H. B. Ahmed, Sizing optimization of a thermoelectric generator set with heat sink for harvesting human body heat, Energy, Convers. Manage., 68 (2013) 260 - 265. https://doi.org/10.1016/j.enconman.2013.01.021

[24] D. Astrain, J.G. Vian, A. Martinez, A. Rodriguez, Study of the influence of heat exchangers' thermal resistances on a thermoelectric generation system, Energy, 35 (2010) 602- 610. https://doi.org/10.1016/j.energy.2009.10.031

[25] F. Meng, L. Chen, F. Sun , Effects of temperature dependence of thermoelectric properties on the power and efficiency of a multielement thermoelectric generator, Int. J. Energy, Environ, 3 (2012) 137-150.

[26] E. F. Thacher, B. T. Helenbrook, M. A. Karri,C. J. Richter, TestingTesting of an automobile exhaust thermoelectric generator in a light truck, Proc. Inst. Mech. Eng. D. J. Auto. Eng., 22 (2007) 95-107. https://doi.org/10.1243/09544070JAUTO51

[27] CT. Hsu, GY. Huang, HS .Chu, B. Yu , DJ. Yao, Experiments and simulations on low temperature waste heat harvesting system by thermoelectric power generators,Appl.Energy,88(2011)1291-1297. https://doi.org/10.1016/j.apenergy.2010.10.005

[28] A. Al-Janabi , O. Alsalmi, E. Alsubhi, A. Alhadhrami, Thermoelectric Generators as a Heat Recovery System for Exhaust Gases of Vehicles Driving at Low Speeds, Eng. Technol. J., 41 (2023) 185-195. https://doi.org/10.30684/etj.2022.134206.1253

[29] N. F. Numan, M. M. Mahdi, M. K. Ahmed, A Comparative Experimental Study Analysis of Solar Based Thermoelectric Refrigerator Using Different Hot Side Heat Sink, Eng. Technol. J., 40 (2022) 90-98. https://doi.org/10.30684/etj.v40i1.2058

[30] C. Suter, Z. R. Jovanovic, A. Steinfeld, A 1 kW thermoelectric stack for geothermal power generation – modeling and geometrical optimization, Appl. Energy, 99 (2012)3 79-385. https://doi.org/10.1016/j.apenergy.2012.05.033

[31] E. S. Mohamed, Experimental study on the effect of active engine thermal management on a bi-fuel engine performance, combustion and exhaust emissions, Appl. Thermal, Eng., 106 (2016) 1352-1365. https://doi.org/10.1016/j.applthermaleng.2016.06.123

[32] E. S. Abdelghany, E. S. Mohamed , H. H. Sarhan, Exhaust heat recovery performance analysis of a Bi-fuel engine utilizing a thermoelectric generation kit and fuel economy evaluation, Case Studies , Thermal, Eng., 49 (2023) 103288. https://doi.org/10.1016/j.csite.2023.103288

[33] Y. D. Deng, T. Hu, C.Q. Su , X. H. Yuan, Fuel Economy Improvement by Utilizing Thermoelectric Generator in Heavy-Duty Vehicle, J. Electron. Mater., 46 (2017) 3227-3234 . https://doi.org/10.1007/s11664-016-4996-1

[34] M. A. Mansour , N. Beithou , A. Othman, A. Qandil , M. B. Khalid , G. Borowski , S. Alsaqoor, A. Alahmer , H. Jouhara, Effect of liquid saturated porous medium on heat transfer from thermoelectric generator, Int. J. Thermofluids., 17 (2023) 100264. https://doi.org/10.1016/j.ijft.2022.100264

[35] P. Ni , R. Hua , H. Jiang , X. Wang , X. Zhang , X. Li , R. Hua, Thermal flow and thermoelectricity characteristics in a sandwich flat plate thermoelectric power generation device under diesel engine exhaust conditions, Energy, 308 (2024) 132815. https://doi.org/10.1016/j.energy.2024.132815

[36] Seebeck, T. J. Magnetische Polarisation der Metalle und Erze Durch Temperatur-Differenz; in Ostwald's Klassiker der Exakten Wissenshaften Nr, Seebeck Biography 1. Seebeck Biography 2, Engelmann, 1895.

[37] M. V. Vedernikov, E. K. Iordanishvili, A. F. Ioffe and origin of modern semiconductor thermoelectric energy conversion, 7th Int. Conf. Thermoelec. Proc., 1 ,1998, 37- 42. https://doi.org/10.1109/ICT.1998.740313

[38] P. Alexandre, S. Susanna , S. Lírio , History of Development of Thermoelectric Materials for Electric Power Generation and Criteria of their Quality, Mat. Res., 17 (2014) 1260-1267. https://doi.org/10.1590/1516-1439.272214